Available online at www.sciencedirect.com

SciVerse ScienceDirect

Journal of the European Ceramic Society 33 (2013) 1001–1008

www.elsevier.com/locate/jeurceramsoc

Piezoelectric and dielectric properties of Ce substituted $La_2Ti_2O_7$ ceramics

Z.P. Gao [a], H.X. Yan [a,b], H.P. Ning [a], R. Wilson [a], X.Y. Wei [b,c], B. Shi [d], H. Ye [d], M.J. Reece [a,b,*]

[a] School of Engineering and Materials Science, Queen Mary University of London, London E1 4NS, UK
[b] Nanoforce Technology Ltd., London E1 4NS, UK
[c] Xi'an JiaoTong University, Xi'an 710049, China
[d] School of Engineering and Applied Science, Aston University, Birmingham B4 7ET, UK

Received 18 September 2012; received in revised form 14 November 2012; accepted 15 November 2012
Available online 14 December 2012

Abstract

The ferroelectric and dielectric properties of cerium (Ce) substituted $La_2Ti_2O_7$ (LTO) have been investigated. Single phase, dense $La_{2-x}Ce_xTi_2O_7$ ($x = 0.15, 0.25, 0.35$) ceramics were prepared by spark plasma sintering. The solubility limit of Ce in $La_{2-x}Ce_xTi_2O_7$ was found to be between 0.35 and 0.5. The *a*-, *b*- and *c*-axes of the unit cell decrease with increasing Ce substitution. The Curie point (Tc) of $La_{2-x}Ce_xTi_2O_7$ ($x = 0$, 0.15, 0.25, 0.35) decreases and dielectric constant and loss increase with increasing Ce substitution. Cerium can increase the d_{33} of $La_2Ti_2O_7$. The highest d_{33} was 3.9 ± 0.1 pC/N for $La_{1.85}Ce_{0.15}Ti_2O_7$ textured ceramic.

Keywords: Ferroelectric; PLS ceramic; Curie point; SPS

1. Introduction

High-temperature piezoelectric sensing technology is of major importance for the chemical and material processing as well as automotive, aerospace, and power generating industries.[1] The commercial materials used for high temperature applications such as tourmaline ($d_{33} \sim 1.8$ pC/N) have relatively low d_{33} compared to lead zirconate titanate (PZT; $d_{33} > 200$ pC/N).[2–4] Ferroelectrics are materials characterized by a Curie point (Tc) and polar structure that can be switched. The Tc corresponds to the ferroelectric–paraelectric transition. Therefore, all ferroelectric materials are limited to operate as piezoelectrics below their Curie point.

Ferroelectrics with perovskite-like layered structure (PLS) are the good candidates for high temperature applications because of their high Curie points (>1200 °C). The PLS family has the general formula of $A_nB_nO_{3n+2}$, with a structure characterized by corner-shared BO_6 octahedra and 12-coordinated A cations within the perovskite-like layers, which are linked by A cations at their boundaries, where *n* is the number of octahedral layers in the perovskite layers.[5,6] When $n = 4$, the compounds have the formula $A_2B_2O_7$, and have been confirmed as ferroelectric materials with super high Curie points, such as $La_2Ti_2O_7$ (LTO, 1461 °C)[7,8]; $Pr_2Ti_2O_7$ (PTO, 1750 °C)[9] and $Nd_2Ti_2O_7$ (NTO, 1482 °C).[8,10]

Of these PLS ceramics, LTO is the most promising for high temperature piezoelectric applications because of its high Curie point (1461 °C)[8] and useful piezoelectric activity.[7,8,11] In the 1970s, the ferroelectric properties of LTO single crystal were characterized.[7,11] It is monoclinic with space group P21, and its lattice constants are (a, b, c, β) = (13.015 Å, 7.817 Å, 5.5456 Å, 98.64°), and the spontaneous polarization is along the *c*-axis. Its piezoelectric constant d_{33} was measured as 16 pC/N.[7,11]

Cerium has similar properties to lanthanum. In $BaTiO_3$ and Aurivillius phase $CaBi_4Ti_4O_{15}$, Ce doping has been reported to increase their high temperature resistivity and piezoelectric constant d_{33}.[12] In some other Aurivillius materials,[13,14] such as $Na_{0.25}K_{0.25}Bi_{2.5}Nb_2O_9$, cerium increases their Curie points.[14] Also, for $Na_{0.5}Bi_{0.5}TiO_3$–$BaTiO_3$, Ce doping increased the dielectric constant at room temperature and the depolarization temperature (T_d).[15] However, there is no reported research on Ce substituted PLS ferroelectric materials. Perovskite-like layered structure (PLS) ceramics can be produced with preferred grain orientation using a two-step hot-forging method.[16,17] In the

* Corresponding author at: School of Engineering and Materials Science, Queen Mary University of London, London E1 4NS, UK.
Tel.: +44 020 7882 8872; fax: +44 18 1981 9804.
E-mail address: m.j.reece@qmul.ac.uk (M.J. Reece).

0955-2219/$ – see front matter © 2012 Elsevier Ltd. All rights reserved.
http://dx.doi.org/10.1016/j.jeurceramsoc.2012.11.015

current work, single phase, dense and textured $La_{2-x}Ce_xTi_2O_7$ ($x = 0.15, 0.25, 0.35$) ceramics were prepared and their properties were characterized.

2. Experimental details

2.1. Sample preparation

The $La_{2-x}Ce_xTi_2O_7$ ($x = 0.15$, 0.25, 0.35, 0.5) compositions (LCTO15, LCTO25, LCTO35, LCTO50) were obtained by the mixed oxide route. La_2O_3 (99.99%), CeO_2 (99.9%) and TiO_2 (99.9%) were used as the starting materials. The powders were milled by ZrO_2 balls with ethanol as the milling medium. Then the powders were calcinated in a normal chamber furnace in air for 4 h at 1300 °C. The powders were re-milled for 4 h to break any agglomerates and reduce the particle size. The ball milling speed was always 350 rpm.

The synthesized powders were sintered in a SPS furnace (HPD 25/1, FCT, Rauenstein, Germany). A heating rate of 100 °C/min was used in all cases. The untextured ceramics used for dielectric tests and Tc measurement were sintered at 1400 °C under a pressure 80 MPa for 5 min.

The textured ceramic samples used for piezoelectric constant measurement (d_{33}) were textured using a two-step sintering method. First, the LCTO15, LCTO25, LCTO35 powders were pressed in a 20-mm-diameter graphite die and sintered at 1200 °C under a pressure of 80 MPa for 3 min. After this stage, all these samples had relatively high density (>95%), but the grain size was only slightly larger than that of the starting powder. In the second step, the samples were placed in a larger die of 30 mm diameter and sintered at 1400 °C under a pressure of 80 MPa for 5 min. The sintered disks were then heat treated in air at 1400 °C for 20 h to anneal and increase grain growth. For the textured ceramics, the orientation of the surface with a normal line perpendicular to the SPS pressing direction is defined as perpendicular sample (⊥) and parallel to SPS pressing direction as parallel (//) (Fig. 1).

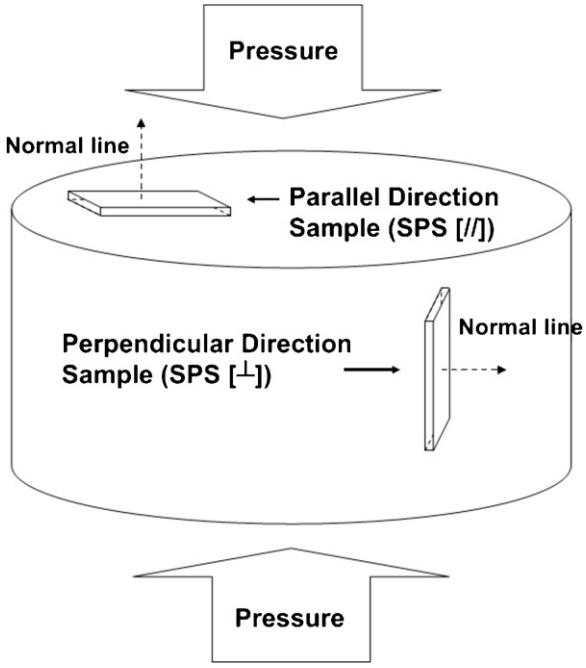

Fig. 1. Diagrammatic sketch of SPS (//) and SPS (⊥) from a bulk ceramic.

2.2. Sample characterization

X-ray diffraction (XRD) patterns for the ceramics were obtained with an X-ray diffractometer (Siemens D5000, Karlsruhe, Germany) using Cu Kα radiation. The microstructures of the ceramic samples were observed using a scanning electron microscope (SEM) (FEI, Inspect F, Hillsboro, OR). The samples for SEM were polished, and then heated to a temperature 110 °C below their sintering temperatures for 30 min in air to etch and reveal their grain structures. The valence state of the elements was determined by the X-ray photoelectron spectroscopy (XPS; ESCALAB MK II, VG Scientific). Carbon was used as the reference material.

Fired-on platinum paste (Gwent Electronic Materials Ltd., C2011004D5, Pontypool, UK) was used to produce the electrodes for the electrical property measurements. The frequency dependence of the dielectric constants and losses were measured using a Precision Impedance Analyzer (Agilent, 4294A, Hyogo, Japan). The temperature dependence of the dielectric constants and losses were measured at different frequencies using a LCR meter (Agilent, 4284A, Hyogo, Japan) connected to a high-temperature furnace. The piezoelectric constant d_{33} was measured using a quasi-static d_{33} meter (CAS, ZJ-3B, Institute of Acoustics Chinese Academy of Sciences, Beijing, China). The accuracy of the d_{33} meter was checked using X-cut quartz ($d_{33} = 2.3 \pm 0.1$ pC/N).[18] The DC resistivity was measured as a function of temperature using an electrometer (Keithley, Model 6517A, Cleveland, OH, USA) with contacts to the samples in a high-temperature furnace. All the resistivity data were recorded after a 15 min holding time at high temperature with a voltage of 10 V (sample thickness ~ 1 mm).

3. Results and discussion

Fig. 1 shows the XRD patterns of the LCTO15, LCTO25, LCTO35 and LCTO50 powders. The diffraction peaks of LCTO15, LCTO25 and LCTO35 match the indexed peaks for the LTO (XRD PDF card: 028-0517) structure parameters, which means that the materials are single phase within the sensitivity of the technique. For LCTO50 there are several XRD peaks that do not match the indexed peaks for LTO, which indicates the solid solution limit for Ce in $La_{2-x}Ce_xTi_2O_7$ is below $x = 0.5$. The impurity is a mixture of Ce_2O_3 and La_2TiO_5.

Fig. 2 shows the change of lattice parameters with increasing Ce substitution determined using the XRD data. The *a*-, *b*- and *c*- dimensions decrease with increasing Ce content. This indicates the Ce substituted into the lattice. All of the compounds have the same structure as LTO, which is monoclinic with space group $P2_1$ at room temperature, and changes into a paraelectric,

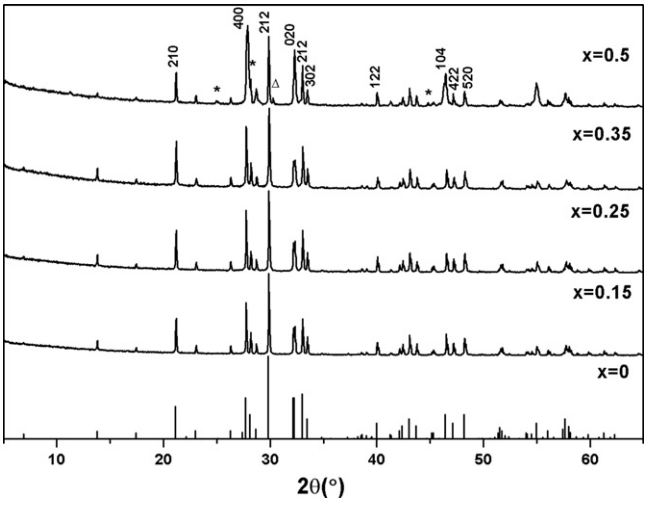

Fig. 2. X-ray diffraction patterns of LCTO15, LCTO25, LCTO35 and LCTO50 powders matching indexed peaks for LTO (XRD PDF card: 00-028-0517). The peaks of Ce_2O_3 (XRD PDF card: 00-078-0484) and La_2TiO_5 (XRD PDF card: 00-0150335) are marked by "Δ" and "*" respectively.

centro-symmetric structure (Cmcm) at the Curie point.[8,19] The spontaneous polarization is along the *c*-axis.[19]

Fig. 3(a)–(d) shows the XPS peaks for the La 3d, Ce 3d, Ti 2p, and O 1s electron binding energies (BE) of the powder samples. The La $3d_{5/2}$ and La $3d_{3/2}$ components show a clear doublet structure for the LCTO15, LCTO25 and LCTO35 samples (Fig. 3(a)). The BE splitting between the components of both La $3d_{5/2}$ and La $3d_{3/2}$ lines is about 4.1 eV. This effect might be due to the interaction between bonding and antibonding states.[20] Comparing these peak positions with the literature data, the La^{3+} state is stable in these materials.[20] The peaks of Ce 3d were compared to reference data for Ce^{3+} and Ce^{4+} compounds (Fig. 3b).[21,22] The $3d_{5/2}$ and $3d_{3/2}$ of Ce^{3+} are split which is also due to the interaction between bonding and antibonding states. Some Ce^{4+} exists in these materials indicated by the peak at 916.5 eV (*). For LCTO15, Ce^{4+} is hardly observed, however, with increasing Ce content, Ce^{4+} peak increases for LCTO25 and LCTO35. The Ti 2p peaks are shown in Fig. 3(c). Compared with the literatures, the Ti^{4+} state is stable and does not change with increasing Ce content.[21,23] Fig. 3(d) shows the peaks for the O 1s state. Two components, A and B, could be identified from the O 1s spectra deconvolution. Component A is about 529.7 eV and component B is at 531.7 eV. Compared to the literature, component A is the O^{2-} in the PLS structure and B with higher BE corresponds to the oxygen connecting Ce^{3+} or point defects.[23,24]

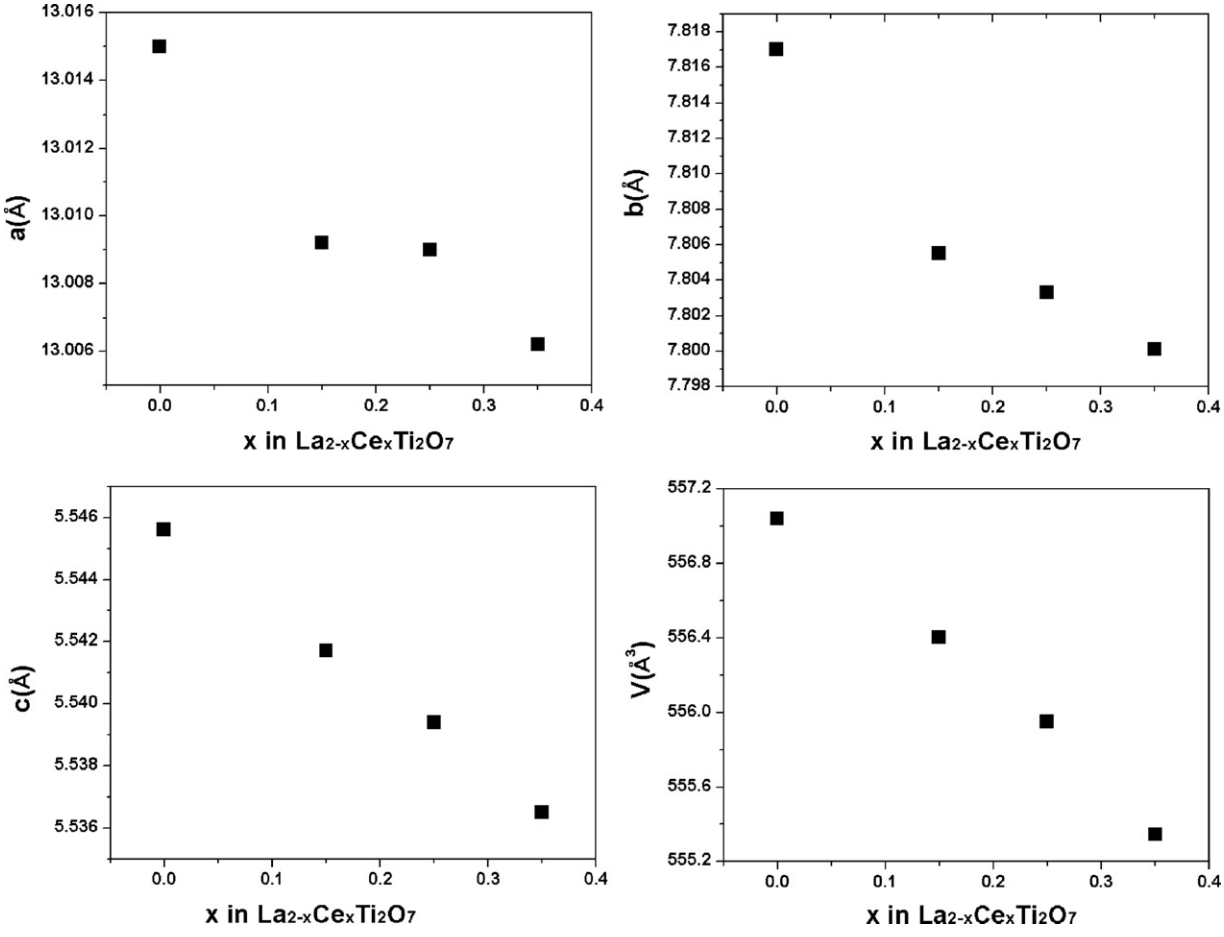

Fig. 3. The lattice parameters of $La_{2-x}Ce_xTi_2O_7$ was function of Ce content.

The data for LTO ($x = 0$) is from Ref. [11].

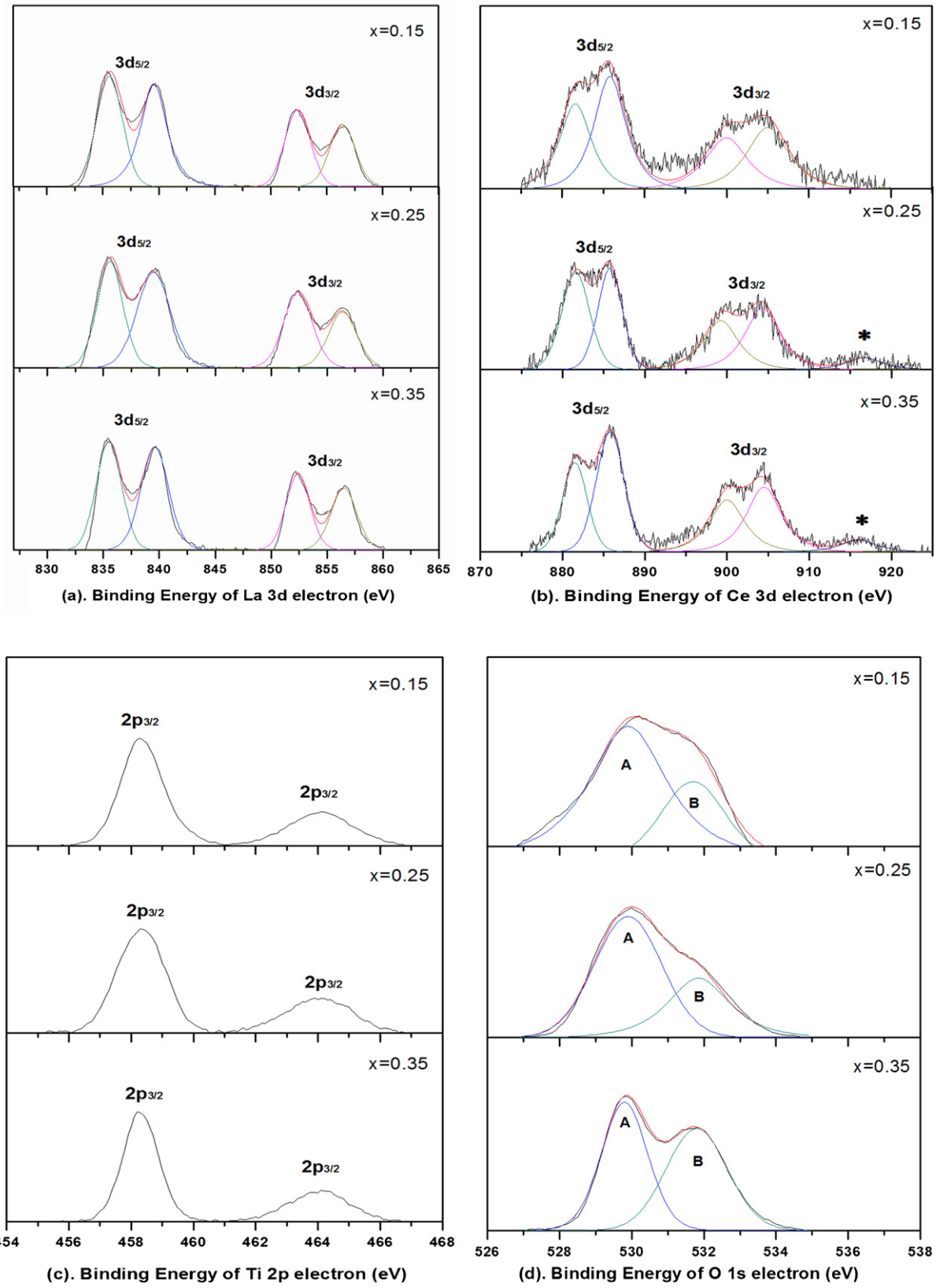

Fig. 4. The X-ray photoelectrons spectroscopy (XPS) peaks of LCTO powder samples for: (a) La 3d; (b) Ce 3d; (c) Ti 2p; and (d) O 1s.

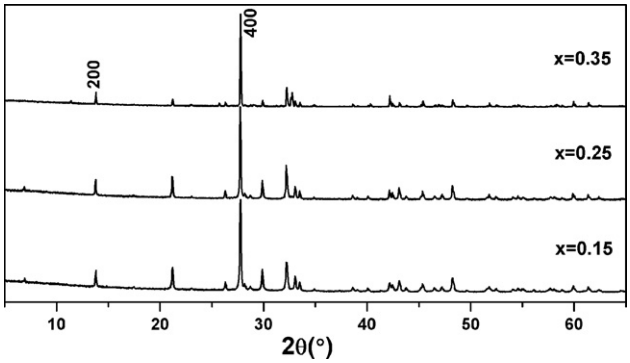

Fig. 5. XRD patterns of textured LCTO ceramics parallel to the pressing direction (//).

Fig. 4 shows the XRD patterns of textured LCTO15, LCTO25, LCTO35 ceramics. The XRD patterns from a plane with its normal direction parallel to the SPS pressing direction exhibit intense ($h\,0\,0$) reflections, which indicates that the ceramics are textured. The Lotgering orientation factor, f, was used to estimate the degree of grain orientation.[25] For LCTO, $f = (P - P_0)/(1 - P_0)$ where $P = \Sigma I(h\,0\,0)/\Sigma I(h\,k\,l)$ and $P_0 = \Sigma I_0(h\,0\,0)/\Sigma I_0(h\,k\,l)$. $\Sigma I(h\,0\,0)$ and $\Sigma I(h\,k\,l)$ are the sum of the XRD peak intensities of all the ($h\,0\,0$) and ($h\,k\,l$) peaks, respectively, for textured LCTO samples over 5–65° of 2θ values. $\Sigma I_0(h\,0\,0)$ and $\Sigma I_0(h\,k\,l)$ are the sum of the XRD intensities of all the ($k\,0\,0$) and ($h\,k\,l$) peaks, respectively, for the powder. The Lotgering factor f of LCTO15, LCTO25, LCTO35 were calculated as 0.71, 0.71, 0.74 for the parallel direction [//].

Fig. 5 shows the SEM micrographs of the polished surfaces of the textured LCTO15, LCTO25 and LCTO35 ceramics viewed perpendicular [⊥] to the SPS pressing direction. The grains prefer to grow along directions perpendicular to the pressing direction. Compared to pure LTO ceramic,[8] the grains become less plate-like due to Ce substitution which explains the low Lotgering orientation factor comparing to LTO (0.80).[8] On average, the plate-like grains are about 1.5 μm in thickness and 5 μm in the other two dimensions for all of the ceramics.

Fig. 6(a)–(c) shows the temperature dependence of the dielectric permittivity (ε) and loss (D) of LCTO15, LCTO25, LCTO35 untextured samples, respectively, measured at two different frequencies, 500 kHz and 1000 kHz. From these figures, the Tc of LCTO15, LCTO25 and LCTO35, are 1440 ± 5 °C, 1435 ± 5 °C, and 1387 ± 5 °C, respectively. The Tc of LTO has previously been reported as 1461 ± 5 °C.[8] With increasing Ce substitution, the Tc decreases gradually. This might be explained by the substituted Ce, which has a smaller ionic size and higher electronegativity compared to La. The inset figs show the temperature dependent loss measured at 100 kHz, 10 kHz and 1 kHz. There are frequency dependence broad peaks could be observed at the temperature range 400–800 °C suggesting that there are point defect in the materials. There are loss peaks just below the Curie point, which are attributed to domain wall movement.[26,27]

Fig. 7 shows the frequency dependence of relative dielectric permittivity and loss of LCTO15, LCTO25 and LCTO35 untextured ceramics measured at room temperature compared with the data for LTO. The loss decreases with increasing frequency. In the lower frequency range (10^3–10^5 Hz), the loss increases with increasing Ce substitution, from LTO to LCTO35. In the higher frequency range (10^5–10^7 Hz) they are similar and low. This behavior may have been produced by the presence of the defect dipoles.[28] This result is consistent with the temperature dependent loss result. The defect dipoles can switch, contributing the loss value in the low frequency range. However, at high frequency the defect dipole cannot follow the electric field change, so the loss decreases to a small value. This behavior is also apparent in the permittivity change, which shows increasing apparent permittivity with decreasing frequency. In comparison, the permittivity of LTO is constant in the whole frequency range. Permittivity increases with increasing amount of Ce substitution. This might be explained by the Ce in the lattice changing the intrinsic dielectric properties.

The DC resistivity of the LTO,[8] LTCO15, LTCO25, LTCO35 untextured ceramics are shown in Fig. 8. Compare to the LTO ceramic, the resistivities of these compounds decrease with increasing Ce content. The inset in Fig. 8 shows the Arrhenius relation between resistivity and temperature which is $p = A\exp(-E_a/kT)$.[29] In the equation, E_a is the activation energy of the current carrier, A is a constant, ρ is the resistivity and k is the Boltzmann constant. For LTO, LCTO15, LTCO25 and LTCO35 ceramics, the activation energies are 1.34, 0.56, 0.53 and 0.52 eV. The band gap of $La_2Ti_2O_7$ is reported as 2.8–3.2 eV.[30] The activation energy for LTO is about half of the band gap, which indicates the DC conductivity is dominated by intrinsic charge carriers. Compared to this, the activation energies of LCTO15, LCTO25 and LCTO35 are much lower. This suggests that the DC conductivities of LCTO15, LCTO25 and LCTO35 are dominated by extrinsic semiconductor charge carriers (n-type)

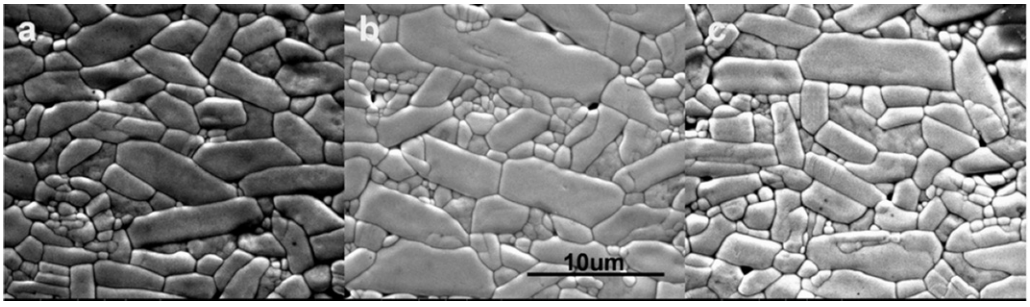

Fig. 6. SEM images of the polished surface viewed perpendicular to the pressing direction (⊥) of the (a) LCTO15; (b) LCTO25; and (c) LCTO35 ceramics.

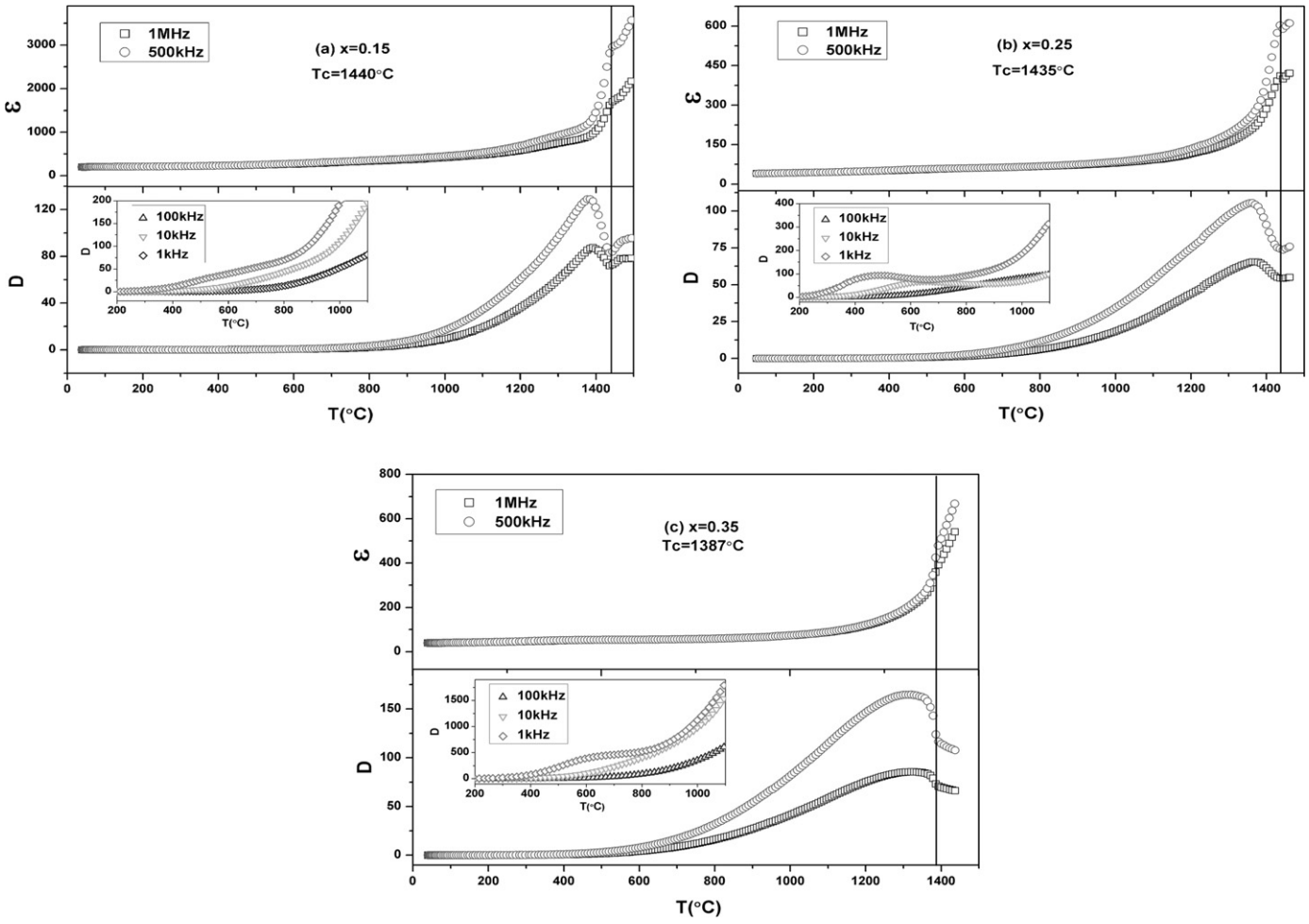

Fig. 7. Temperature dependence of the dielectric constant and loss of LCTO untextured ceramics at different frequencies of 1 MHz and 500 kHz. The inset figs are the data for temperature dependence loss measured at 100 kHz, 10 kHz and 1 kHz.

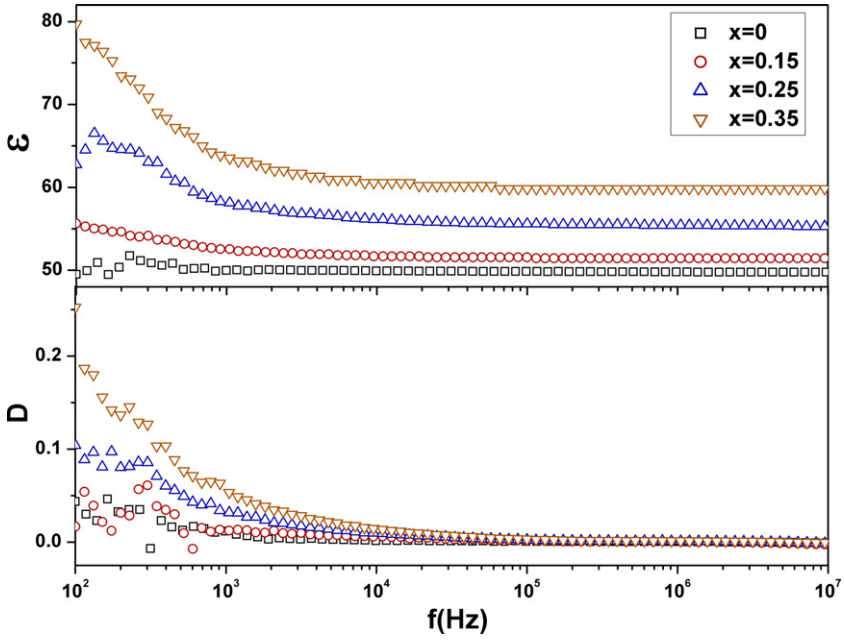

Fig. 8. Frequency dependence of dielectric constant and loss of untextured ceramics of LTO,[8] LCTO15, LCTO25, and LCTO35.

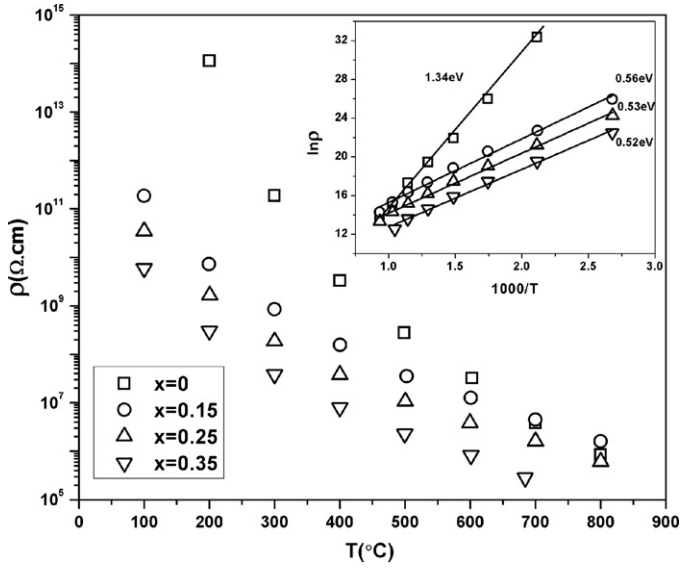

Fig. 9. Direct-current electric resistivity of LTO,[8] LCTO15, LCTO25 and LCTO35 ceramics. The inset is the Arrhenius relation between resistivity and temperature.

produced by the donor dopant,[31,32] which is consistent with the results of XPS. For piezoelectric sensor application, the resistivity should be high, but the Ce lower the resistivity of LCTO15 compare to LTO at 100 °C. However, the resistivity of LCTO15 is still high and similar to LTO at about 800 °C.

The piezoelectric constant d_{33} was measured in a direction perpendicular to pressing direction (Fig. 9). The textured samples were poled in silicone oil at 120 °C under various DC electric fields. The highest electric fields that could be achieved during poling were 19 kV/mm, 19 kV/mm and 16 kV/mm for LCTO15, LCTO25 and LCTO35 respectively. The addition of $x = 0.15$ Ce increased the d_{33} (LCTO15, 3.9 ± 0.1 pC/N) compared to LTO (2.6 ± 0.1 pC/N) poled at 20 kV, 220 °C, which has even higher density (>98%) and Lotgering orientation factor

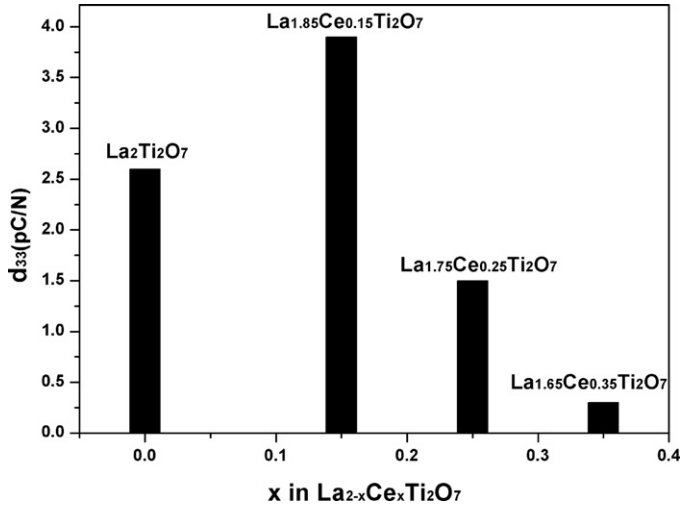

Fig. 10. Piezoelectric constant (d_{33}) of the textured ceramics measured perpendicular to the pressing direction (⊥).
The data for LTO is from Ref. [8].

($f = 0.80$).[8] With further increasing Ce substitution, the d_{33} decreased from LCTO15 to LCTO35. This is because the defect concentration increases and resistivity decreases with increasing Ce substitution, leading to a reduction in the maximum poling field that could be applied (Fig. 10).

4. Conclusion

Single phase, dense $La_{2-x}Ce_xTi_2O_7$ ($x = 0$, 0.15, 0.25, 0.35) ceramics were prepared by spark plasma sintering. The limit of Ce substitution in $La_{2-x}Ce_xTi_2O_7$ was found to be between 0.35 and 0.50. The *a*-, *b*- and *c*-axes of the unit cell decrease with increasing Ce content, which indicates that Ce substitutes into the lattice. The Curie points (Tc) of $La_{2-x}Ce_xTi_2O_7$ ($x = 0$, 0.15, 0.25, 0.35) decrease and dielectric constant and loss increase with increasing Ce substitution. Electrical resistivity decreases due to the extrinsic charge carriers produced by Ce substitution. The highest d_{33} was 3.9 ± 0.1 pC/N for $La_{1.85}Ce_{0.15}Ti_2O_7$.

Acknowledgment

Z. P. Gao would thank China Scholarship Council for supporting his PhD studies.

References

1. Kimura T. Application of texture engineering to piezoelectric ceramics – a review. *J Ceram Soc Jpn* 2006;**114**:15–25.
2. Zhang S, Yu F. Piezoelectric materials for high temperature sensors. *J Am Ceram Soc* 2011;**94**:17–34.
3. Saito Y, Takao H, Tani T, Nonoyama T, Takatori K, Homma T, et al. Lead-free piezoceramics. *Nature* 2004;**432**:84–7.
4. Frayssignes H, Gabbay M, Fantozzi G, Porch NJ, Cheng BL, Button TW. Internal friction in hard and soft PZT-based ceramics. *J Eur Ceram Soc* 2004;**24**:2989–94.
5. Lichtenberg F, Herrnberger A, Wiedenmann K. Synthesis, structural, magnetic and transport properties of layered perovskite-related titanates, niobates and tantalates of the type $A_nB_nO_{3n+2}$, $A'A_{k-1}B_kO_{3k+1}$ and $A_mB_{m-1}O_{3m}$. *Prog Solid State Chem* 2008;**36**:253–387.
6. Lichtenberg F, Herrnberger A, Wiedenmann K, Mannhart J. Synthesis of perovskite-related layered $A_nB_nO_{3n+2} = ABO_X$ type niobates and titanates and study of their structural, electric and magnetic properties. *Prog Solid State Chem* 2001;**29**:1–70.
7. Nanamats S, Kimura M, Yamada N. Ferroelectric properties of $La_2Ti_2O_7$ crystal. *NEC Res Dev* 1974;**34**:39–42.
8. Yan H, Ning H, Kan Y, Wang P, Reece M. Piezoelectric ceramics with super-high curie points. *J Am Ceram Soc* 2009;**92**:2270–5.
9. Gao Z, Yan H, Ning H, Reece M. Ferroelectricity of $Pr_2Ti_2O_7$ ceramics with super-high curie point. *Adv Appl Ceram*, http://dx.doi.org/10.1179/1743676112Y.0000000030, in press.
10. Kimura M, Nanamats S, Kawamura I, Matsushi S. Ferroelectric, electrooptic and piezoelectric properties of $Nd_2Ti_2O_7$ single crystal. *Jpn J Appl Phys* 1974;**13**:1473–4.
11. Nanamats S, Kimura M, Doi K, Matsushi S, Yamada N. New ferroelectric – $La_2Ti_2O_7$. *Ferroelectrics* 1974;**8**:511–3.
12. Yan H, Zhang Z, Zhu W, He L, Yu Y, Li C, et al. The effect of (Li,Ce) and (K,Ce) doping in Aurivillius phase material $CaBi_4Ti_4O_{15}$. *Mater Res Bull* 2004;**39**:1237–46.
13. Huang Z, Guo S, Cai Z, Li Y, Wang G, Dong X. Conduction of (Na, Ce) doped $Bi_5Ti_3FeO_{15}$ ceramics after different annealing processes. *Adv Appl Ceram*, http://dx.doi.org/10.1179/1743676112Y.0000000054, in press.
14. Gai Z, Wang J, Wang C. Effect of (Li,Ce) doping in Aurivillius phase material $Na_{0.25}K_{0.25}Bi_{2.5}Nb_2O_9$. *Appl Phys Lett* 2007;**90**, 052911-4.

15. Babu J, He M, Zhang D, Chen X, Dhanasekaran R. Enhancement of ferroelectric properties of $Na_{1/2}Bi_{1/2}TiO_3$–$BaTiO_3$ single crystals by Ce dopings. *Appl Phys Lett* 2007;**90**, 102901-3.
16. Yan H, Ning H, Zhang H, Reece M. Textured high Curie point piezoelectric ceramics prepared by spark plasma sintering. *Adv Appl Ceram* 2010;**109**:139–42.
17. Hao J, Wang X, Chen R, Gui Z, Li L. Preparation of textured bismuth titanate ceramics using spark plasma sintering. *J Am Ceram Soc* 2004;**87**:1404–6.
18. Janghorb M, Freund H. Application of a piezoelectric quartz crystal as a partition detector – development of digital sensor. *Anal Chem* 1973;**45**:325–32.
19. Ishizawa N, Marumo F, Iwai S, Kimura M, Kawamura T. Compounds with perovskite-type slabs. 5: a high-temperature modification of $La_2Ti_2O_7$. *Acta Crystallogr* 1982;**38**:368–72.
20. Atuchin V, Gavrilova T, Grivel J, Kesler V. Electronic structure of layered ferroelectric high-*k* titanate $La_2Ti_2O_7$. *J Phys D: Appl Phys* 2009;**42**:1404–6.
21. Beche E, Charvin P, Perarnau D, Abanades S, Flamant G. Ce 3d XPS investigation of cerium oxides and mixed cerium oxide ($Ce_xTi_yO_z$). *Surf Interface Anal* 2008;**40**:264–7.
22. Charvin P, Abanades S, Beche E, Lemont F, Flamant G. Hydrogen production from mixed cerium oxides via three-step water-splitting cycles. *Solid State Ionics* 2009;**180**:1003–10.
23. Chu M, Ganne M, Caldes M, Brohan L. X-ray photoelectron spectroscopy and high resolution electron microscopy studies of Aurivillius compounds: $Bi_{4-x}La_xTi_3O_{12}$ ($x = 0$, 0.5, 0.75, 1.0, 1.5, and 2.0). *J Appl Phys* 2002;**91**:3178–87.
24. Shah L, Ali B, Zhu H, Wang W, Song Y, Zhang H, et al. Detailed study on the role of oxygen vacancies in structural, magnetic and transport behavior of magnetic insulator: Co–CeO_2. *J Phys: Condens Matter* 2009;**21**:486004.
25. Lotgering F. Topotactical reaction with ferromagnetic oxides having hexagonal crystal structures. I. *J Inorg Nucl Chem* 1959;**9**:113–23.
26. Gerthsen P, Hardtl K, Schmidt N. Correlation of mechanical and electrical losses in ferroelectric ceramics. *J Appl Phys* 1980;**51**:1131–4.
27. Pertsev N, Arlt G, Zembilgotov A. Domain-wall and intrinsic contributions to the dielectric response of epitaxial ferroelectric films. *Microelectron Eng* 1995;**29**:135–40.
28. Park S, Han Y. Dielectric relaxation of oxygen vacancies in Dy-doped $BaTiO_3$. *J Korean Phys Soc* 2010;**57**:458–63.
29. Ngai K, Greaves G, Moynihan C. Correlation between the activation energies for ionic conductivity for short and long time scales and the Kohlrausch stretching parameter β for ionically conducting solids and melts. *Phys Rev Lett* 1998;**80**:1018–21.
30. Bruyer E, Sayede A. Density functional calculations of the structural, electronic, and ferroelectric properties of high-*k* titanate $Re_2Ti_2O_7$ (Re = La and Nd). *J Appl Phys* 2010;**108**:053705.
31. Kudo T, Obayashi H. Mixed electrical-conduction in fluorite-type $Ce_{1-x}Gd_xO_{2-x/2}$. *J Electrochem Soc* 1976;**123**:415–9.
32. Jaiswal N, Singh N, Kumar D, Parkash O. Effect of strontium (Sr) doping on the conductivity of ceria. *J Power Sources* 2012;**202**:78–84.